Break-Up of Stepped Platinum Catalyst Surfaces by High CO Coverage

Feng Tao, *et al.*

Science **327**, 850 (2010);
DOI: 10.1126/science.1182122

observed link ratios of those MTV-MOFs synthesized from an equimolar ratio of links involving the most sterically unencumbered link A, where a disproportionately higher amount of link A is retained in the resulting MTV-MOFs (Table 1).

The possible presence of distinct sequences of functionalities along the MOF backbone would inevitably lead to a complex pore environment and provide opportunities for uncovering unusual properties. Because the same-link MOF-5 structure can take up large amounts of gases (for example, H_2, CO_2) (*8*, *11*–*13*), we sought to test the MTV-MOFs in these applications and to determine whether their performance is greater than that of their constituents. In Fig. 2A, we compare the H_2 storage capacities of MTV-MOF-5-AHI, -AH, -AI, and MOF-5. The isotherms demonstrate that the uptake capacity of MTV-MOF-5-AHI is greater than that of MTV-MOF-5-AH, -AI, and -A (MOF-5) by a maximum of 84%. Similarly, an unusual increase in the selective uptake capacity of CO_2 over CO was observed: 400% better selectivity in the case of MTV-MOF-5-EHI for CO_2 compared with MOF-5 (*4*, *14*, *15*) (Fig. 2B). These findings demonstrate that the properties of MTV-MOFs are not simple linear combinations of their constituents, thus supporting the notion that the sequence of functionalities within MTV-MOF may very well be useful as code for the enhancement of a specific property or achieving a new property.

References and Notes

1. S. B. Darling, *Prog. Polym. Sci.* **32**, 1152 (2007).
2. R. Kitaura, K. Fujimoto, S. Noro, M. Kondo, S. Kitagawa, *Angew. Chem. Int. Ed.* **41**, 133 (2002).
3. K. Kumazawa, K. Biradha, T. Kusukawa, T. Okano, M. Fujita, *Angew. Chem. Int. Ed.* **42**, 3909 (2003).
4. R. Banerjee *et al.*, *Science* **319**, 939 (2008).
5. K. Koh, A. G. Wong-Foy, A. J. Matzger, *Angew. Chem. Int. Ed.* **47**, 677 (2008).
6. A. D. Burrows, C. G. Frost, M. F. Mahon, C. Richardson, *Angew. Chem. Int. Ed.* **47**, 8482 (2008).
7. S. J. Garibay, Z. Wang, K. K. Tanabe, S. M. Cohen, *Inorg. Chem.* **48**, 7341 (2009).
8. H. Li, M. Eddaoudi, M. O'Keeffe, O. M. Yaghi, *Nature* **402**, 276 (1999).
9. M. Eddaoudi *et al.*, *Science* **295**, 469 (2002).
10. See supporting online material on *Science* Online.
11. N. L. Rosi *et al.*, *Science* **300**, 1127 (2003).
12. S. S. Kaye, A. Dailly, O. M. Yaghi, J. R. Long, *J. Am. Chem. Soc.* **129**, 14176 (2007).
13. A. R. Millward, O. M. Yaghi, *J. Am. Chem. Soc.* **127**, 17998 (2005).
14. R. Banerjee *et al.*, *J. Am. Chem. Soc.* **131**, 3875 (2009).
15. Single-link MOFs of links H and I, respectively, were synthesized and found to be nonporous. Furthermore, we were unable to synthesize a single-link MOF from link E; thus, CO_2/CO separation data for these compounds was not included in our comparison.

16. This work was supported by DOE Office of Basic Energy Sciences (grant DE-FG02-08ER15935). We thank F. J. Uribe-Romo and R. Taylor for assistance and helpful discussions. MTV-MOF-5-AC and MTV-MOF-5-ACEF have been deposited into the Cambridge Crystallographic Data Centre (CCDC) under deposition numbers CCDC 747004 to 747007.

Supporting Online Material

www.sciencemag.org/cgi/content/full/327/5967/846/DC
Materials and Methods
Figs. S1 to S52
Tables S1 to S20
References

10 September 2009; accepted 30 November 2009
10.1126/science.1181761

Break-Up of Stepped Platinum Catalyst Surfaces by High CO Coverage

Feng Tao,[1,2] Sefa Dag,[3] Lin-Wang Wang,[3] Zhi Liu,[4] Derek R. Butcher,[1,2] Hendrik Bluhm,[4,5] Miquel Salmeron,[1,6]* Gabor A. Somorjai[1,2]*

Stepped single-crystal surfaces are viewed as models of real catalysts, which consist of small metal particles exposing a large number of low-coordination sites. We found that stepped platinum (Pt) surfaces can undergo extensive and reversible restructuring when exposed to carbon monoxide (CO) at pressures above 0.1 torr. Scanning tunneling microscopy and photoelectron spectroscopy studies under gaseous environments near ambient pressure at room temperature revealed that as the CO surface coverage approaches 100%, the originally flat terraces of (557) and (332) oriented Pt crystals break up into nanometer-sized clusters and revert to the initial morphology after pumping out the CO gas. Density functional theory calculations provide a rationale for the observations whereby the creation of increased concentrations of low-coordination Pt edge sites in the formed nanoclusters relieves the strong CO-CO repulsion in the highly compressed adsorbate film. This restructuring phenomenon has important implications for heterogeneous catalytic reactions.

Industrial catalysts usually consist of small particles exposing different atomic terminations that exhibit a high concentration of step edges, kink sites, and vacancies at the edge of the facets, which are thought to be the catalytically active sites (*1*–*3*). Stepped single-crystal surfaces with well-defined surface structures can be prepared with a high density of such sites. They are models of real catalysts because vicinal surfaces mimic closely the rough regions of the catalyst surface.

Adsorbates are known to induce structural changes, known as reconstructions in surface science. Steps are particularly notable for being modified when adsorbates bind to the surface. These are phenomena well known in vacuum surface science (*4*–*6*). The present work deals with more profound changes, driven by the formation of dense adsorbate layers. These can be formed when the adsorption energy is high—for example, when oxygen adsorbs and initiates the oxidation process. When the adsorption energy is weaker, however, dense layers can only be formed under reaction conditions of high reactant pressures near or above room temperature.

Real catalysts operate under pressures ranging from millitorr to atmospheres and from room temperature to hundreds of degrees Celsius, so that the surfaces can easily change and adopt the structure corresponding to thermodynamic equilibrium. However, most surface science experiments are usually performed under high vacuum where the high adsorbate coverage characteristic of working catalysts cannot be attained unless the samples are kept at low temperature. These conditions will likely inhibit any restructuring process that requires overcoming of even moderate activation barriers. Thus, to understand catalytic processes at the atomic and molecular level, it is crucial to explore the structural and chemical evolution of catalyst surfaces under reaction conditions.

The limitations of traditional surface science techniques can be overcome with the use of techniques that operate under realistic conditions (*7*–*13*), including high-pressure scanning tunneling microscopy (STM) and ambient pressure x-ray photoelectron spectroscopy (AP-XPS). With these two techniques, we can image the atomic structure and identify the chemical state of catalyst atoms and adsorbed reactant molecules under realistic conditions. Here we concentrate on carbon monoxide (CO), a reactant in many important industrial catalytic processes, such as Fischer-Tropsch synthesis of hydrocarbons (*14*, *15*), CO oxidation in automobile catalytic converters (*16*, *17*), and degradation of Pt electrodes in hydrogen fuel cell processes (*18*–*20*).

Our studies revealed an unexpected and reversible large-scale restructuring of the surfaces of two Pt stepped surfaces, Pt(557) and Pt(332), both of which consist of six-atoms-wide terraces of (111) orientation separated by monoatomic steps of different orientation. On Pt(557) the step atoms form a (100)-type square cell, whereas on Pt(332) they form a (111)-type triangular cell (fig. S1) (*21*). Under high coverage of CO, these flat terraces break up into an array of nanoclusters

[1]Materials Science Division, Lawrence Berkeley National Lab, Berkeley, CA 94720, USA. [2]Department of Chemistry, University of California, Berkeley, CA 94720, USA. [3]Computational Research Division, Lawrence Berkeley National Lab, Berkeley, CA 94720, USA. [4]Advanced Light Source, Lawrence Berkeley National Lab, Berkeley, CA 94720, USA. [5]Chemical Science Division, Lawrence Berkeley National Lab, Berkeley, CA 94720, USA. [6]Department of Materials Science and Engineering, University of California, Berkeley, CA 94720, USA.

*To whom correspondence should be addressed. E-mail: somorjai@berkeley.edu (G.A.S.); mbsalmeron@lbl.gov (M.S.)

aligned along the step directions. Density functional theory (DFT) calculations were performed to help elucidate the energetics and the mechanisms underlying the restructuring from steps and flat terraces to nanoclusters.

Representative images of the Pt(557) under ultrahigh-vacuum conditions (base pressure 1×10^{-10} torr), under ~5×10^{-8} torr of CO, and under 1 torr of CO are shown in Fig. 1. When CO was introduced in the reactor cell at low pressure, the initially straight steps (Fig. 1A) became wavy (Fig. 1B). The STM images also revealed a doubling of terrace width and step height on the Pt(557) surface (figs. S2B and S3B) (*21*). On Pt(332) the step edges did not increase their roughness under the same pressure conditions, a result that we ascribe to the different atomic packing of the Pt(332) and Pt(557) steps (fig. S1, A and B) (*21*). More dramatic effects occurred when the CO pressure was increased to 0.1 torr and higher. The terraces on Pt(557) broke down into nanoclusters about 2.2 nm by 2.1 nm in size, along [1-12] and [110] directions (Fig. 1C).

The nanoclusters have a roughly triangular shape with the vertex pointing to the lower terrace (Fig. 1, C and D). On Pt(332) the nanoclusters are rectangular or roughly parallelogram shaped (fig. S4B) (*21*), a difference in geometry that is probably related to the different step structure of the surfaces. Line profiles indicate that on Pt(557) the nanoclusters in adjacent terraces are separated by 4.2 Å, i.e., two atoms in height (fig. S2D) (*21*), whereas neighboring nanoclusters in the same terrace are separated by ~2 Å deep gaps, i.e., a single atom.

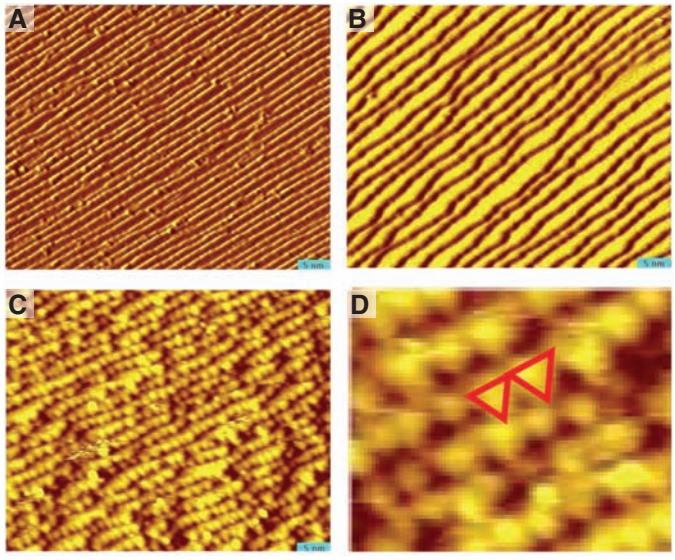

Fig. 1. STM images of Pt(557) (**A**) in ultrahigh vacuum with a background pressure of 1×10^{-10} torr; (**B**) under ~5×10^{-8} torr of CO; and (**C**) under 1 torr of CO. Images are 40 nm by 50 nm in size. (**D**) Enlarged view of (C) showing the roughly triangular shape of the nanoclusters formed at 1 torr. Two of the clusters are marked with red lines.

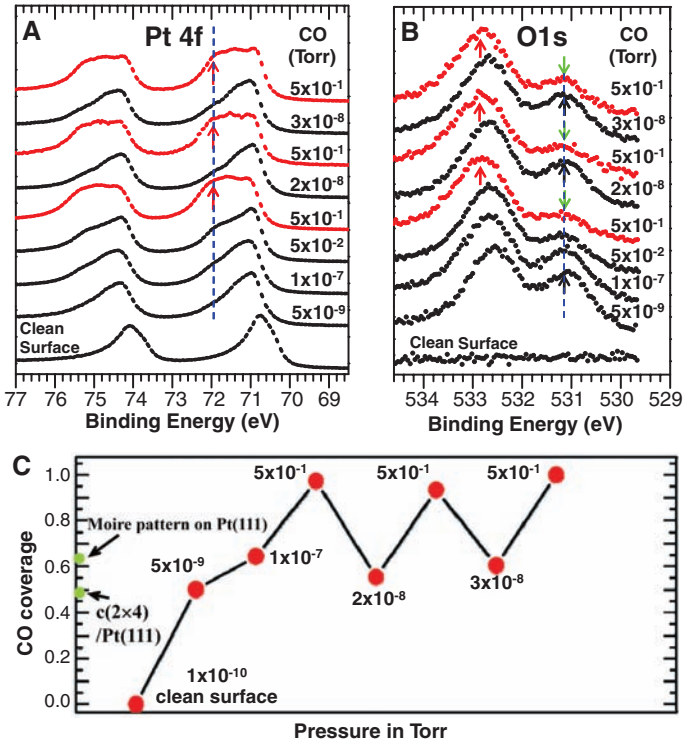

Fig. 2. Photoemission spectra of the Pt4f (**A**) and O1s core levels (**B**) acquired with 340- and 800-eV x-rays, respectively, under different CO pressures. Binding energies were referenced to the Fermi level measured under the same conditions. The red spectra were obtained at 5×10^{-1} torr. The red and green arrows in (A) and (B) mark the increase of photoemission intensity in the high–binding energy side of the $Pt4f_{7/2}$ and the simultaneous decrease of intensity in the low–binding energy side of the O1s spectra, respectively, at high pressure. The black arrows in (B) mark the relatively larger photoemission intensity in the low–binding energy side at low pressure, compared to that at high pressure. (**C**) Coverage of CO on Pt(557) under different pressures as determined from the photoemission peak areas calibrated with the published 0.5 coverage of CO in the low-pressure c(2 × 4) structure at 5×10^{-9} torr.

With increasing CO coverage, the relative intensity of the O1s peak at 532.6 eV (top sites) and 531.0 eV (bridge sites) decreased, whereas there is a substantial build-up of intensity at 533.1 eV (red arrows in Fig. 2B), as the CO pressure increased to 5×10^{-1} torr. This peak is attributed to CO bound to low-coordinated Pt sites. The reversible changes of the Pt4f and O1s photoemission features as the CO pressure changed from high (5×10^{-1} torr) to low (2×10^{-8} or 3×10^{-8} torr) (Fig. 2) agrees with the reversibility of the morphological changes in the surface structure. Indeed, the nanoclusters form and disappear as the pressure is cycled between high and low values, as shown in fig. S6 (*21*). A similar reversible formation of nanoclusters was observed on Pt(332).

XPS allows us to determine the coverage of CO as a function of pressure (Fig. 2C). On Pt(557), the high-pressure coverage is 1.94 times that at low pressure (5×10^{-9} torr). Using the coverage of 0.5 for CO in the c(2 × 4) adsorption layer on Pt(322), Pt(355), and Pt(111) (*23*–*25*) at 5×10^{-9} torr at room temperature, we calibrated the XPS peak areas and found the coverage of CO on Pt(557) to be 0.97 at 5×10^{-1} torr. The coverage decreased to ~0.5 after the CO was pumped out, and increased again to 0.93 after the CO was reintroduced to 5×10^{-1} torr. Similarly, the CO coverage on Pt(332) at high pressure increased by 0.3 to 0.4 relative to that at low pressure (10^{-9} to 10^{-7} torr), and it alternately increased and decreased at high pressure and low pressure (fig. S10) (*21*). Such dramatic changes in real-space structure, shown by STM, and core-level binding energies, shown by XPS, between

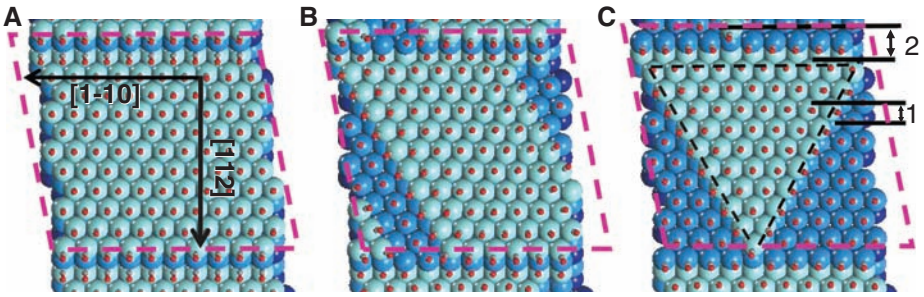

Fig. 3. Models of double-stepped Pt(557) surface covered by CO at high pressure used in the DFT calculations: (**A**) unrestructured terrace, (**B**) parallelogram-shaped nanoclusters, and (**C**) triangular-shaped nanoclusters. Dashed line frames in each image show the periodic supercell used in the DFT calculations. First- and second-layer Pt atoms are represented with olive green and blue balls, respectively. Red dots represent the oxygen atoms of CO molecules. In (C), 1 and 2 indicate step edge heights (one or two Pt atoms).

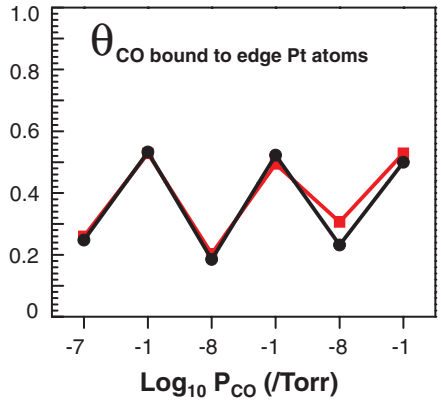

Fig. 4. Coverage of CO molecules adsorbed on low-coordination sites as a function of pressure. The red curve is the coverage calculated with the O1s peak component at 533.1 eV [D in fig. S5 (*21*)]. For the black curve, we used Pt4f peak component C in fig. S5 (*21*).

high and low pressure on Pt(557) and Pt(332) were not observed on Pt(111) by XPS (fig. S7) (*21*) or by STM (*25*).

The restructuring of steps upon CO adsorption at low pressure (step height doubling, kink formation) is due to changes in the energetics of the electronic and elastic step-step interaction, as has been discussed extensively (*4*–*6*). The more dramatic changes observed at higher pressure must be related to the very high coverage of CO, one molecule per surface Pt atom, which cannot be achieved under vacuum. This high density should result in a strong repulsion between CO molecules. We thus propose that the observed break-up of the surface is driven by the relaxation of the repulsive CO-CO interaction, which is facilitated by the formation of nanoclusters. Such restructuring provides a substantial increase in the number of low-coordinated edge atoms where CO molecules can tilt away from the center and thus decrease their mutual repulsion. We found also that this broken-up surface is active for CO oxidation even at room temperature (*26*), possibly because of a low activation barrier for CO desorption at the very high coverage.

DFT calculations were done using the experimentally observed surface structure and CO coverage as starting points. In the low-pressure regime ($<10^{-3}$ torr), a c(2 × 4) CO adlayer with a coverage of 0.5 on the flat terraces was assumed, while at 0.1 torr or higher, a full CO layer with a coverage of 1 was assumed. Calculations were carried out on a clean surface with single-atom height steps, on a surface with double terrace widths and double-atom height steps, and on a surface restructured with triangular- and parallelogram-shaped clusters. To compare energies, we used the chemical potentials of Pt and CO to account for possible differences in the number of atoms and molecules in different systems with the same surface area. Whereas the Pt chemical potential is just the bulk binding energy, the CO chemical potential was calculated from the pressure-dependent gas-phase entropy (*21*). On the clean Pt(557) surface, the single-atom height step structure is energetically more favorable than the double-atom height one by 0.12 eV per edge atom [table S1 (*21*)]. The double-width terrace structure is energetically more favorable by 0.40 eV per edge atom upon adsorption of CO in a c(2 × 4) layer, consistent with the experimental observations (Fig. 1, A and B). In contrast to Pt(557), calculations show that on Pt(332), the surface with double-atom step heights is not more stable upon CO adsorption, again in agreement with the experimental results.

For the high-pressure (1 × 1) CO layer on Pt(557), we calculated the total free energy of the three structures shown in Fig. 3: a flat double terrace (A), a parallelogram created by removing two rows of Pt atoms (B), and a triangle nanocluster spanning the width of the terrace (C). For the double terrace [fig. S3B (*21*)], whether the CO molecules are adsorbed on Pt atoms at the bottom of the steps [A1 in fig. S3B (*21*)] or not gives a slightly different total energy. The calculation shows that covering the step-down side will reduce the total free energy by 0.144 eV per atom. This difference is much smaller than the adsorption energy of CO on the nanoclusters. Thus, as shown in Fig. 3, each Pt atom in the step-down side adsorbs one CO molecule in the models. The total free energies of these three systems (table S2) show that the structure with triangular nanoclusters has the lowest energy, followed by the parallelogram, and then by the flat double terrace. In the final structure after relaxation, the CO molecules adsorbed at the edge of the nanoclusters fan out considerably. This binding configuration reduces the repulsion between adjacent CO molecules and therefore decreases the energy. The increased density of low-coordinated Pt sites and coverage of CO molecules bound to such sites at high pressure (≥0.1 torr) (*27*) is consistent with the Pt4f and O1s photoemission peak structure. For example, the coverage of CO molecules bound to low-coordinated sites in the nanoclusters is ~53% at 0.1 torr or higher (*28*) and 20 to 24% at 2×10^{-8} to 1.1×10^{-7} torr (Fig. 4) (*29*).

The occurrence of large-scale surface restructuring of stepped Pt crystals highlights the strong connection between coverage of reactant molecules and atomic structure of the catalyst surface under reaction conditions. These results have important implications for catalysis where high pressures and high coverage of reactant molecules on the catalyst surfaces are the norm.

References and Notes

1. G. Ertl, H. Knözinger, F. Schüth, J. Weitkamp, *Handbook of Heterogeneous Catalysis* (VCH-Wiley, Weinheim, Germany, 2008).
2. G. A. Somorjai, *Introduction to Surface Chemistry and Catalysis* (VCH-Wiley, Weinheim, Germany, 1997).
3. C. Burda, X. Chen, R. Narayanan, M. A. El-Sayed, *Chem. Rev.* **105**, 1025 (2005).
4. J. C. Dunphy *et al.*, *Surf. Sci.* **280**, 313 (1993).
5. J. D. Batteas, J. C. Dunphy, G. A. Somorjai, M. Salmeron, *Phys. Rev. Lett.* **77**, 534 (1996).
6. T. P. Pearl, S. J. Sibener, *J. Chem. Phys.* **115**, 1916 (2001).
7. F. Tao, D. Tang, M. Salmeron, G. A. Somorjai, *Rev. Sci. Instrum.* **79**, 084101 (2008).
8. D. F. Ogletree *et al.*, *Rev. Sci. Instrum.* **73**, 3872 (2002).
9. M. Salmeron, R. Schlögl, *Surf. Sci. Rep.* **63**, 169 (2008).
10. H. Bluhm *et al.*, *MRS Bull.* **32**, 1022 (2007).
11. F. Tao *et al.*, *Science* **322**, 932 (2008).
12. P. L. Hansen *et al.*, *Science* **295**, 2053 (2002).
13. P. Nolte *et al.*, *Science* **321**, 1654 (2008).
14. J. M. Thomas, W. J. Thomas, in *Principles and Practices of Heterogeneous Catalysis* (VCH-Wiley, Weinheim, Germany, 1997), chap. 8.
15. T. Herranz, X. Deng, A. Cabot, J. Guo, M. Salmeron, *J. Phys. Chem. B* **113**, 10721 (2009).
16. X. W. Xie, Y. Li, Z. Q. Liu, M. Haruta, W. Shen, *Nature* **458**, 746 (2009).
17. T. Bär, T. V. de Bocarmé, B. E. Nieuwenhuys, N. Kruse, *Catal. Lett.* **74**, 127 (2001).
18. J. A. Rodriguez *et al.*, *Science* **318**, 1757 (2007).
19. W. B. Kim, T. Voitl, G. J. Rodriguez-Rivera, J. A. Dumesic, *Science* **305**, 1280 (2004).
20. Q. Fu, H. Saltsburg, M. Flytzani-Stephanopoulos, *Science* **301**, 935 (2003).
21. Supporting material is available on *Science* Online.
22. O. Björneholm *et al.*, *Surf. Sci.* **315**, L983 (1994).
23. B. Tränkenschuh *et al.*, *J. Chem. Phys.* **124**, 074712 (2006).
24. B. Tränkenschuh, C. Papp, T. Fuhrmann, R. Denecke, H. Steinruck, *Surf. Sci.* **601**, 1108 (2007).
25. S. R. Longwitz *et al.*, *J. Phys. Chem. B* **108**, 14497 (2004).
26. CO_2 was detected by means of a quadrupole mass spectrometer installed in the second pumping stage of the XPS lens system.
27. The coverage of CO molecules bound to Pt atoms at the edge of the triangular nanoclusters used in the DFT calculation is 0.5 (Fig. 3C); the overall coverage of CO on the surface with triangular nanocluster (Fig. 3C) is 1.
28. The ratio of the O1s peak area from CO bound to low-coordinated Pt atoms to the total peak area of the O1s

peak at 0.5 torr is 0.55, and the overall CO coverage is 0.97. The coverage of CO molecules bound to low-coordinated Pt atoms is defined as the ratio of the number of CO molecules adsorbed at low-coordinated Pt atoms to the number of surface Pt atoms.
29. The ratio of the O1s peak area from CO bound to low-coordinated Pt atoms to the total peak O1s area of CO at 10^{-8} to 10^{-7} torr is 0.35 to 0.40; the overall CO coverage at this pressure is ~0.56.
30. The experimental work was supported by the director, Office of Basic Energy Sciences, Materials Sciences, and Chemical, Geosciences, and Biosciences Divisions. The theoretical work was supported by the Office of Advanced Scientific Computing Research. U.S. Department of Energy under Contract No. DE-AC02-05CH11231. The computation uses the resources of National Energy Research Scientific Computing Center (NERSC) and the INCITE project allocations within the National Center for Computational Sciences (NCCS). XPS data were collected at the Advanced Light Source, Berkeley, CA.
F.T. acknowledges the discussions with S. L. Bernasek, N. Kruse, T. Bligaard, and F. Ogletree.

Supporting Online Material
www.sciencemag.org/cgi/content/full/327/5967/850/DC1
Materials and Methods
SOM Text
Figs. S1 to S13
Tables S1 and S2
References

17 September 2009; accepted 24 December 2009
10.1126/science.1182122

Quantum-State Controlled Chemical Reactions of Ultracold Potassium-Rubidium Molecules

S. Ospelkaus,[1]* K.-K. Ni,[1]* D. Wang,[1] M. H. G. de Miranda,[1] B. Neyenhuis,[1] G. Quéméner,[1] P. S. Julienne,[2] J. L. Bohn,[1] D. S. Jin,[1]† J. Ye[1]†

How does a chemical reaction proceed at ultralow temperatures? Can simple quantum mechanical rules such as quantum statistics, single partial-wave scattering, and quantum threshold laws provide a clear understanding of the molecular reactivity under a vanishing collision energy? Starting with an optically trapped near–quantum-degenerate gas of polar $^{40}K^{87}Rb$ molecules prepared in their absolute ground state, we report experimental evidence for exothermic atom-exchange chemical reactions. When these fermionic molecules were prepared in a single quantum state at a temperature of a few hundred nanokelvin, we observed p-wave–dominated quantum threshold collisions arising from tunneling through an angular momentum barrier followed by a short-range chemical reaction with a probability near unity. When these molecules were prepared in two different internal states or when molecules and atoms were brought together, the reaction rates were enhanced by a factor of 10 to 100 as a result of s-wave scattering, which does not have a centrifugal barrier. The measured rates agree with predicted universal loss rates related to the two-body van der Waals length.

Scientific interest in precisely understanding the fundamental aspects of chemical reactions and controlling their dynamic processes has stimulated pioneering work on molecular beams to study state-to-state reactions using molecular alignment, velocity selections, and angle-resolved measurement (*1*–*5*). However, substantial motional energies remained in earlier work, and thermal statistical averages were a necessary ingredient. By preparing a molecular ensemble's translational degrees of freedom in the quantum regime, we expect to develop fundamental insights into how chemical reaction processes may be precisely guided by quantum mechanics. Reaction dynamics at vanishingly low energies remain a fascinating and yet unexplored scientific realm (*6*). Under unprecedented energy resolution, each step of a complex reaction may be analyzed on the basis of single quantum states and single reaction channels. For example, we can study how reactivity is dictated by the quantum statistics of the molecule as a whole.

That chemical reactions could occur at ultralow temperatures seems at first glance counterintuitive. However, ultracold collisions, where particles scatter only in the partial wave with lowest angular momentum, are governed by quantum statistics and quantum threshold behaviors described by the Bethe-Wigner laws (*7*–*9*). In this regime, particles are represented by their de Broglie wavelength, which increases with reduced temperature. This wave nature of particles replaces our intuitive and classical picture of collisions. The wave manifestation of tunneling through reaction or angular momentum barriers may play a dominant role in dynamics, and scattering resonances can have dramatic effects on reactions (*10*). In addition, any barrierless chemical reactions will always take place when two reactants are sufficiently close together (*11*). In this case, chemical reaction rates will be determined to a large extent by collisional properties at large intermolecular separations, and thus by how the two partners approach each other. Once their separation reaches a characteristic length scale (~$10a_0$, where $a_0 = 0.53 \times 10^{-10}$ m), a chemical reaction happens with a near unity probability. Therefore, chemical reactions can be surprisingly efficient even at ultracold temperatures. Indeed, this model for barrierless reactions predicts loss rates that are universal in the sense that they do not depend on the details of the short-range interactions, but instead can be estimated using only knowledge of the long-range interactions (*12*).

Like the case of collisions of ultracold atoms, the study of ultracold chemical reactions will play a fundamental role in advancing the field of molecular quantum gases. For example, understanding and manipulating collisions of atoms at ultralow temperatures (<1 μK) has been crucial for the realization of quantum degenerate gases (*13*–*15*), Fermi superfluids that provide opportunities to explore the underlying connection between superconductivity and Bose-Einstein condensation (*16*), neutral atom–based systems for quantum information science (*17*–*19*), and strongly correlated quantum gases (*20*, *21*). Ultracold molecules undergo a more diverse set of collisional processes, with distinct inelastic collision mechanisms arising from chemical reactions, in addition to the traditional state-changing collisions seen with ultracold atoms and highly vibrationally excited molecules (*22*). Furthermore,

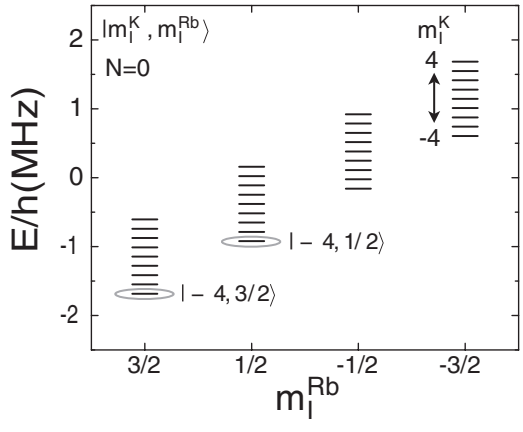

Fig. 1. Hyperfine structure of rovibronic ground-state $^{40}K^{87}Rb$ molecules at 545.9 G. We label the 36 nuclear spin states by their spin projections, m_I^{Rb} and m_I^K. The energy spacing between hyperfine states is ~h × 130 kHz for $|\Delta m_I^K| = 1$ and ~h × 760 kHz for $|\Delta m_I^{Rb}| = 1$. By comparison, at a temperature of 300 nK, the molecules' thermal energy is equivalent to ~h × 6 kHz, which is more than an order of magnitude smaller than the spin flip energy. In our experiments, molecules are prepared in either a single state or in a mixture of $|-4,1/2\rangle$ and the lowest-energy state $|-4,3/2\rangle$ (open ellipses).

[1]JILA, NIST and University of Colorado, Department of Physics, University of Colorado, Boulder, CO 80309, USA. [2]Joint Quantum Institute, NIST and University of Maryland, Gaithersburg, MD 20899, USA.

*These authors contributed equally to this work.
†To whom correspondence should be addressed. E-mail: jin@jilau1.colorado.edu (D.S.J.); ye@jila.colorado.edu (J.Y.)